BOLETÍN DE LA SOCIEDAD ESPAÑOLA DE CERÁMICA Y VIDRIO XXX (2021) XXX–XXX

BOLETIN DE LA SOCIEDAD ESPAÑOLA DE
Cerámica y Vidrio
www.elsevier.es/bsecv

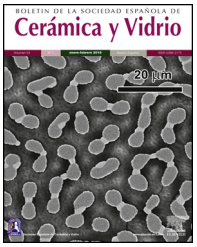

Original

Fabrication and characterization of high entropy pyrochlore ceramics

Branko Matović[a,*], *Dejan Zagorac*[a], *Ivana Cvijović-Alagić*[a], *Jelena Zagorac*[a], *Svetlana Butulija*[a], *Jelena Erčić*[a], *Ondrej Hanzel*[b], *Richard Sedlák*[c], *Maksym Lisnichuk*[d], *Peter Tatarko*[b]

[a] *Centre of Excellence "CEXTREME LAB", Vinča Institute of Nuclear Sciences – National Institute of the Republic of Serbia, University of Belgrade, Mike Petrovica Alasa 12-14, 11000 Belgrade, Serbia*
[b] *Institute of Inorganic Chemistry, Slovak Academy of Sciences, Dúbravská cesta 9, 84536 Bratislava, Slovak Republic*
[c] *Institute of Materials Research, Slovak Academy of Sciences, Watsonova 47, 04001 Košice, Slovak Republic*
[d] *Faculty of Science, Institute of Physics, Pavol Jozef Šafárik University in Košice, Park Angelinum 9, 04001 Košice, Slovak Republic*

ARTICLE INFO

Article history:
Received 3 September 2021
Accepted 10 November 2021
Available online xxx

Keywords:
High-entropy ceramics
Pyrochlore structure
Densification
Crystal structure prediction

ABSTRACT

High-entropy rare-earth (RE) zirconates with pyrochlore structure were successfully fabricated by pressureless and spark plasma sintering. $RE_2Zr_2O_7$ compound with nominal composition $(La_{0.2}Y_{0.2}Gd_{0.2}Nd_{0.2}Sm_{0.2})Zr_2O_7$ was prepared by simple glycine nitrate procedure (GNP). GNP process yielded powders with low crystallinity and after subsequent calcination, well crystalline ceramics were formed. During calcination defective fluorite (F-$RE_2Zr_2O_7$) and crystal pyrochlore (Py-$RE_2Zr_2O_7$) structures coexist. Formation of pure crystalline pyrochlore occurs after sintering at 1450 °C. High-density ceramics, free of any additives, were obtained after powders compaction and pressureless (PS), as well as field assisted sintering technique (FAST) at 1450 °C. Theoretical investigations of the high-entropy $RE_2Zr_2O_7$ pyrochlore systems were performed. Unit cell parameter of the obtained Py-$RE_2Zr_2O_7$ is 10.5892(2) Å and 10.5999(2) Å for PS and FAST sintering, respectively, which is in good agreement with the results of Density Functional Theory (DFT) calculations. The thermal diffusivity of sintered samples at room temperature was ~0.7 mm^2/s for both sintering methods.

Fabricación y caracterización de cerámicas de pirocloro de alta entropía

Palabras clave:
Cerámica de alta entropía
Estructura de pirocloro
Densificación
Predicción de la estructura cristalina

RESUMEN

Se fabricaron con éxito, mediante sinterización por plasma sin presión y por chispa, los circonatos de tierras raras (RE) de alta entropía con estructura de pirocloro. El compuesto $RE_2Zr_2O_7$ con composición nominal $(La_{0,2}Y_{0,2}Gd_{0,2}Nd_{0,2}Sm_{0,2})Zr_2O_7$ se preparó mediante un procedimiento simple de nitrato de glicina (GNP). El proceso GNP produjo polvos con baja cristalinidad y después de la posterior calcinación, se formaron cerámicas bien cristalinas.

* *Corresponding author.*
E-mail address: mato@vinca.rs (B. Matović).
https://doi.org/10.1016/j.bsecv.2021.11.002

Please cite this article in press as: B. Matović, et al., Fabrication and characterization of high entropy pyrochlore ceramics, Bol. Soc. Esp. Cerám. Vidr. (2021), https://doi.org/10.1016/j.bsecv.2021.11.002

Durante la calcinación coexisten estructuras defectuosas de fluorita (F-$RE_2Zr_2O_7$) y pirocloro cristalino (Py-$RE_2Zr_2O_7$). La formación de pirocloro cristalino puro se produce después de la sinterización a 1.450 °C. Después de la compactación de polvos y sin presión (PS), así como por la técnica de sinterización asistida en campo (FAST) a 1.450 °C, se obtuvieron cerámicas de alta densidad, libres de aditivos. Se realizaron investigaciones teóricas de los sistemas de pirocloro $RE_2Zr_2O_7$ de alta entropía. El parámetro de celda unitaria del Py-$RE_2Zr_2O_7$ obtenido es 105.892(2) Å y 105.999(2) Å para la sinterización PS y FAST, respectivamente, lo que está de acuerdo con los resultados de los cálculos de la teoría funcional de la densidad (DFT). La difusividad térmica de las muestras sinterizadas a temperatura ambiente fue de ~ 0,7 mm^2/s para ambos métodos de sinterización.

Introduction

Compounds based on the $A_2B_2O_7$ general formula, where A and B are metals, represent a family of phases isostructural to the pyrochlore mineral. When the structure is concerned, the pyrochlore shows $Fd\bar{3}m$ crystal structure, which describes materials of the $A_2B_2O_6$ and $A_2B_2O_7$ types in which the A and B species are generally rare-earth (RE) or transition metal species [1]. Its structure is a superstructure derivative of the simple fluorite structure ($AO_2 = A_4O_8$), where the A and B cations are ordered along the ⟨110⟩ direction (space group 227), and it is very close to the disordered fluorite structure (space group 225) [1].

In compounds with the space group 227, the A-site cation is ordinarily occupied by larger trivalent 8-coordinated cation, typically rare-earth elements, while the B-site represents the smaller tetravalent 6-coordinated cation of transition metals, i.e. Ti, Zr, Hf [1–3].

Not only the structure but also the properties of these compounds are highly dependent on the composition and the ratio of radii of A-site cation (rA^{3+}) and B-site cation (rB^{3+}). The stability of pyrochlores is governed by the radius ratio between the A- and B-site cations [4–7]. The pyrochlore-type structure is experimentally observed for radius ratio rA^{3+}/rB^{4+} in the range from 1.46 to 1.78. When the cation radius ratio is higher than 1.78 a monoclinic perovskite with layered structure is preferred, while for a ratio lower than 1.46 a distorted fluorite structure is favored [1].

Due to different combinations of A and B cations sites, pyrochlores possess a wide range of various chemical and physical properties such as thermal conductivity [8,9], nuclear waste storage capacity [10], neutron absorption [11], ionic conductivity [12,13], geometrically frustrated magnetism [14], luminescence [15,16], photocatalysis [17], that could be controlled by changing the constituent ions. The other very attractive method for obtaining pyrochlore with novel or improved properties is the high-entropy concept. The focus of high-entropy pyrochlores (HEPy) synthesis is on complex element compositions, in which many cations are doped onto one site [18]. The structure can accept the chemical substitution of a wide variety of elements on the cation and anion sites. Two different types of doping for pyrochlores are common: (1) substitutional doping onto the A- or B-sites, (2) antisite doping of A/B-site cations onto the B/A-sites [18–24].

Numerous methods can be used to fabricate different pyrochlore materials, such as solid-state reaction method [25], sol–gel method [26], solid-state displacement reaction [27], a combination of sol–gel processing and complex precipitation [28], mechanical milling [29] and molten salt reaction [30], combustion synthesis [31], precipitation method [32], hydrothermal route [33], atmospheric plasma spraying [34], *etc.* Bearing in mind that among all of these various methods the glycine nitrate process (GNP) method was successfully used for the synthesis of a significant number of oxides [15] it is believed that this method could be also effectively employed for the synthesis of high-entropy pyrochlores powders.

In this paper, the high-entropy design concept is employed to fabricate five rare-earth metal zirconate ceramics. Firstly, the formation of the variable compositions of ordered and disordered pyrochlore structures was investigated using a combination of quantum mechanics and group-theoretical analysis. In the experimental part, the GNP method for pyrochlore materials obtainment was selected in the present research as it provides excellent mixing of constituent elements in the liquid state allowing the formation of the final, crystalline, product after thermal treatment at relatively low temperature [35]. The phase evolution during calcination, as well as sinterability of the obtained powders, were studied along with crystallinity of the final phase in the sintered body.

Materials and methods

Theoretical studies

Pyrochlore structures were generated using the Primitive Cell Approach for Atom Exchange (PCAE) method [36] or the supercell approach using the Crystal17 program package [37,38], and investigation of disordered systems and solid solutions was conducted using the group action theory [39]. Structural optimization on the *ab initio* level was performed using the Crystal17 code, based on a Linear Combination of Atomic Orbitals (LCAO) [37,38].

Density functional theory (DFT) calculations were utilized in the present study, using the local density approximation (LDA) with Perdew–Zunger (PZ) correlation functional [40]. In particular, effective core pseudopotential (ECP) for lanthanum labeled La_ECP_Heifets_2013 [41,42] was used together with the ECP for gadolinium labeled Gd_ECP_Doll_2008 [43]

Please cite this article in press as: B. Matović, et al., Fabrication and characterization of high entropy pyrochlore ceramics, Bol. Soc. Esp. Cerám. Vidr. (2021), https://doi.org/10.1016/j.bsecv.2021.11.002

and ERD_SmallCore_2017 [44]. An all-electron basis set (AEBS) labeled buljan_1999 for yttrium [45], the ECP pseudopotential for samarium labeled Sm_ERD_ SmallCore_2017 [44], the ECP pseudopotential for neodymium labeled Nd_ERD_ SmallCore_2017 [44], the AEBS basis set for oxygen [46–48], and in the case of zirconium the ECP pseudopotential by Hay and Wadt labeled Zr_ECP_HAYWSC_311d31G_dovesi_1998 [49] were applied in all calculations. For the integration over the Brillouin zone, a k-point mash of $8 \times 8 \times 8$ was generated using the Monkhorst–Pack scheme [50]. To analyze the symmetry of the calculated structures, the SFND algorithm [51] and RGS algorithm [52] implemented in the KPLOT software package [53] were used. Investigated pyrochlore structures were visualized using the VESTA program [54].

Experimental procedure

Materials and synthesis

Starting chemicals used for the synthesis of high-entropy pyrochlore powders were glycine, zirconium chloride, and RE nitrates hexahydrates (RE = La, Y, Nd, Gd, Sm). All precursors were used in the as-received forms. The synthesis was carried out in a stainless-steel reactor in which all reactants were dissolved in distilled water and added according to the previously calculated composition of the final powder. The synthesis reaction was proposed according to the following equation:

$$\begin{aligned} &2RE(NO_3)_3 \cdot 6H_2O + 2ZrCl_4 + 4NH_2CH_2COOH + 3O_2 \\ &= (La_{0.2}Y_{0.2}Gd_{0.2}Nd_{0.2}Sm_{0.2})_2\,Zr_2O_7 + 5H_2 + 8CO_2 \\ &+ 18H_2O + 8HC1\,(39\,mol\,of\,gases/mol\,of \\ &(La_{0.2}Y_{0.2}Gd_{0.2}Nd_{0.2}Sm_{0.2})_2\,Zr_2O_7) \end{aligned} \quad (1)$$

where RE states for La, Y, Gd, Nd, Sm. The reaction (1) is presented in its simplified form since this reaction is taking place in multiple stages, which is explained elsewhere [6].

The mixture of solutions was heated in a laboratory furnace, where the reaction after ignition proceeds spontaneously and terminates extremely fast at about 450 °C with the strong release of gaseous products in accordance with the reaction (1). As a result, the ash powder was obtained. Calcination of the obtained ash was undertaken to burn out organic components and produce a clean homogeneous oxide powder of the desired stoichiometry. The obtained powder was calcined for 120 min at a temperature ranging from 950 to 1350 °C. Synthesized powders were uniaxially compacted at 200 MPa without any binder into disks with 15 mm in diameter and 5 mm thickness. Samples were conventionally sintered in a furnace at 1450 °C. The heating rate was 10 °C/min while the soaking time was 4 h. The other technique used in the present study for the densification of as-synthesized pyrochlore powders was the field assisted sintering technique (FAST) for spark plasma sintering (SPS) conducted at 1450 °C for 5 min using a pressure of 70 MPa in an argon atmosphere. The heating and cooling rates were 100 and 50 °C/min, respectively. During the present study, the conventional and FAST sintering processes were conducted at the same sintering temperature of 1450 °C to obtain pyrochlore samples with comparable characteristics.

Materials characterization

The phase analysis of calcined powders was accomplished by X-ray diffraction (XRD) using RIGAKU Ultima IV diffractometer with filtered Cu Kα radiation (1.54178 nm) in the 2θ range from 20° to 80°. The present phases were identified using the PDXL2 software (version 2.0.3.0), with reference to the patterns of the International Centre for Diffraction Data (ICDD) [55], version 2012.

The microstructure and chemical composition of the sintered samples was studied by field-emission scanning electron microscopy (FE-SEM) using the S-4800 FE-SEM microscope, Hitachi, Japan, operated at 20 keV coupled with the INCA x-site energy dispersive spectrometer (EDS), Oxford Instruments, UK. Also, the microstructure of the SPS-sintered sample was studied by transmission electron microscopy (TEM) utilizing the JEOL JEM 2100 microscope, JEOL, Akishima, Japan, with LaB_6 electron source operated at 200 kV in a scanning mode (STEM). The TEM imaging samples were prepared by grinding, dimpling, and Ar-ion thinning.

Raman spectra of the polished FAST-sintered high-entropy pyrochlore sample were recorded using the DXR Raman Microscope, Thermo Fisher Scientific Inc., USA, equipped with an Ar laser operating at 532 nm irradiation wavelength. Fifteen Raman spectra were recorded under the same operating conditions at different positions of the SPS-sintered sample to confirm a homogenous structure of the sample.

The thermal diffusivity of sintered samples was measured by the laser flash technique using the LFA 1000, Linseis, Germany, from room temperature up to 200 °C with a step of 100 °C in a nitrogen atmosphere. The thermal diffusivity measurements were conducted in the mentioned temperature range due to the expected low thermal diffusivity of the obtained samples at higher temperatures. Prior to the measurement, a thin layer of graphite was sprayed onto both sides of the sintered pyrochlore samples to hinder any reflection of the laser beam or the sensitivity of the infrared sensor on the backside of samples. At least three measurements were done at each temperature and the mean values were calculated.

The densities of all sintered samples were measured by the Archimedes method. The theoretical density of 15.84 g/cm^3 was calculated based on the crystal structure of pyrochlore with the space group 227 and the proportional ratio of cations according to the desired nominal composition.

The microhardness of the sintered samples was determined using the Vickers indentation hardness tester model Buehler Identamet 1114, Buehler, Germany, by applying a load of 1 kgf (9807 mN) for 15 s. The microhardness values were determined at 10 measuring points of each sample with excellent reproducibility.

Results and discussion

Theoretical investigations of the $RE_2Zr_2O_7$ pyrochlore systems

Theoretical methods were applied to investigate the variable composition of the ordered and disordered pyrochlore structures using quantum mechanics, group action theory, PCAE, and supercell methods. The experimentally observed

Please cite this article in press as: B. Matović, et al., Fabrication and characterization of high entropy pyrochlore ceramics, Bol. Soc. Esp. Cerám. Vidr. (2021), https://doi.org/10.1016/j.bsecv.2021.11.002

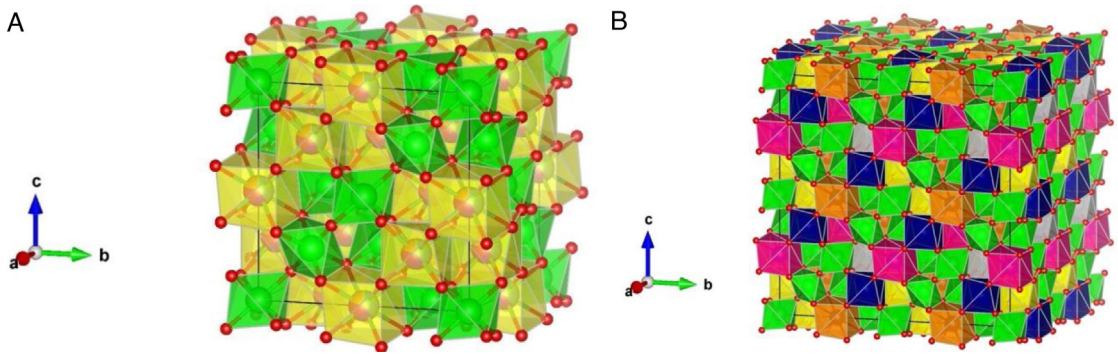

Fig. 1 – (a) Ordered pyrochlore structure obtained from the recorded XRD data, (b) model of ordered pyrochlore structure generated using the 2 × 2 × 2 supercell. Lanthanum atoms/polyhedra are presented in yellow color, yttrium in blue, gadolinium in gray, samarium in purple, neodymium in orange, zirconium in green, and oxygen atoms in red color.

$(La_{0.2}Y_{0.2}Gd_{0.2}Nd_{0.2}Sm_{0.2})_2Zr_2O_7$ compound crystallizes in the cubic $Fd\bar{3}m$ (no. 227) space group as parent pyrochlore structure $La_2Zr_2O_7$, where La atoms are located at 16d, Zr atoms at 16c, and O atoms at 48f and 8b Wyckoff positions. The PCAE method was applied to create various doped $La_2Zr_2O_7$ compositions. The primitive cell consists only of four lanthanum atoms, with only one symmetry irreducible active site, out of four active sites (see Table A.1 in Appendix A), resulting in five possible compositions for La substitutions: 0%, 25%, 50%, 75%, and 100%. If zirconium atoms are additionally substituted on the B cation position, together with La atoms, the number of possibilities increases to nine compositions and a total of eight active crystallographic sites (see Table A.2 in Appendix A). Moreover, the total number of symmetry independent classes of composition increases to 35, *e.g.* for 87.5% of lanthanum at A cation position (equals to 7 La atoms) there is one lanthanum atom that can be substituted on A cation position or one Zr atom that can be replaced on the B cation position creating 2 symmetry independent classes of compounds, *etc.* (see Table A.2 in Appendix A).

A large number of supercell structures were created to investigate the variable composition of ordered and disordered pyrochlore structures. By constructing the $2 \times 2 \times 2$ supercell of pyrochlore structure, the number of La atoms sites are increased to 32, but with only one symmetry irreducible active site (see Table A.3 in Appendix A). The number of possible compositions is largely increased to 33, however, the total number of symmetry independent classes of composition was dramatically increased to 11.251.322 possible chemical systems. Some additional interesting supercell structures are presented in the supporting information given in Appendix A (Appendix Asee Tables A.4 and A.5 in Appendix A).

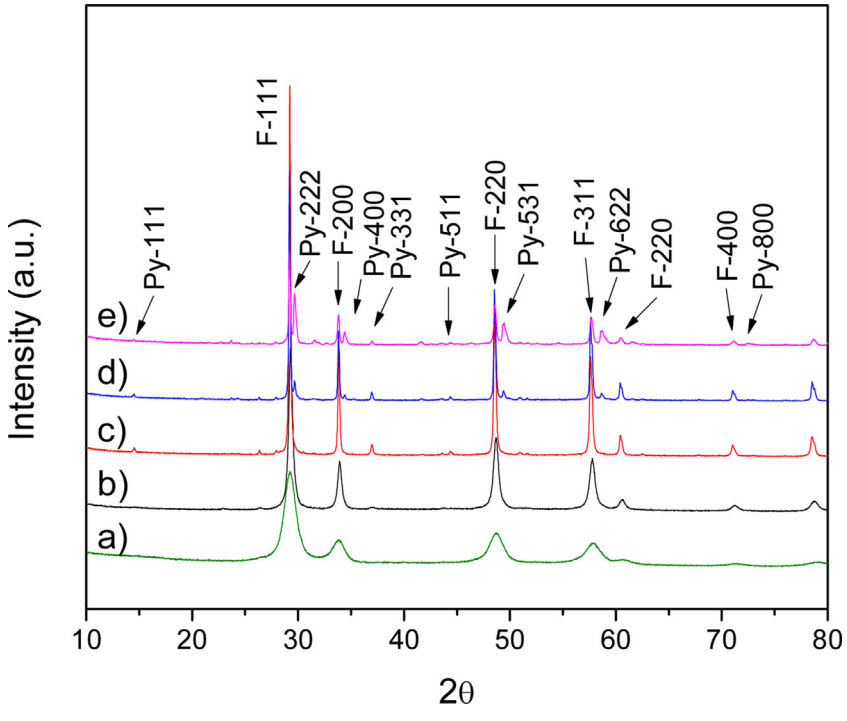

Fig. 2 – Calcined (La, Gd, Nd, Sm, Y)$_2$Zr$_2$O$_7$ powders treated at different temperatures for 2 h: (a) 950 °C, (b) 1050 °C, (c) 1150 °C, (d) 1250 °C and (e) 1350 °C.

Please cite this article in press as: B. Matović, et al., Fabrication and characterization of high entropy pyrochlore ceramics, Bol. Soc. Esp. Cerám. Vidr. (2021), https://doi.org/10.1016/j.bsecv.2021.11.002

Fig. 1a shows experimentally observed ordered pyrochlore structure, with partial occupancy on La (16d) Wyckoff position sharing eightfold coordinated polyhedra with 20% of Y, Gd, Nd, and Sm, respectively, while Zr atoms are in the sixfold coordinated octahedral environment. By generating the $2 \times 2 \times 2$ supercell a full occupancy of the La, Y, Gd, Nd, and Sm atoms at A cation position was obtained, Fig. 1b. After structural optimization on the DFT level within this supercell, calculated unit cell parameters were slightly underestimated from the XRD results (<2%) which is in agreement with previous calculations using LDA functional [56,57] (additional structures for various compositions are presented in Fig. A.1 as supporting information given in Appendix A). These results show a strong indication that these variable composition order/disorder pyrochlore systems are particularly susceptible to geometrical frustrations in agreement with previous research on pure and doped order/disorder pyrochlore structures [20,58–70]. Present experimental and theoretical results for doped pyrochlore structures might have numerous practical applications, from oxygen conductors with improved NO_2 sensing performance [71] to photocatalyst materials for environmental and energy applications [72].

XRD analysis

Typical XRD patterns of powders calcined at different temperatures for 2 h are shown in Fig. 2.

The XRD pattern of the sample calcined at 950 °C exhibits very broad diffraction lines indicating its low crystallinity state. The strongest reflection, located around ~29°, can be assigned to the {111} reflection of the defect fluorite structure. Also, the other reflections correspond to the fundamental fluorite structure with the 225 space group: *F*{200}, *F*{220}, *F*{311}. However, at higher temperatures, calcination temperature causes narrowing of the diffraction lines and increasing of their intensities, which is the result of increased crystallite size. The powders thermally treated at 1150 °C show that in addition to the defective fluorite-type structure, the phase with the pyrochlore type structure also appears. A new phase exhibits an ordered pyrochlore type structure, which is characterized by the presence of typical superstructure diffraction peaks at the 2θ values of 14° {111}, 37° {331}, 45° {511}, and 51° {531} using Cu Kα radiation [73].

The thermal treatment at 1450 °C showed that densities of 93% and 98% of theoretical density can be achieved for pressureless and FAST sintering, respectively. Generally speaking, the success of powders consolidation is closely related to the control of the competition between densification and coarsening. In the case of pressureless sintering, it can be observed that at a temperature of 1450 °C the maximal achieved density was 93%. On the other hand, it was noted that the density for the FAST-sintered sample at the same temperature of 1450° C was 98%. The green structure, *i.e.* pore size distribution, plays an important role in the achievement of high density. Densification is retarded or inhibited for wide pore distribution. In such a case, big pores became larger while small pores shrank. The SPS-sintered samples show much better results when densities are concerned compared with the conventionally sintered one, despite the short sintering time of 5 min. The XRD patterns of these samples depicted that both obtained

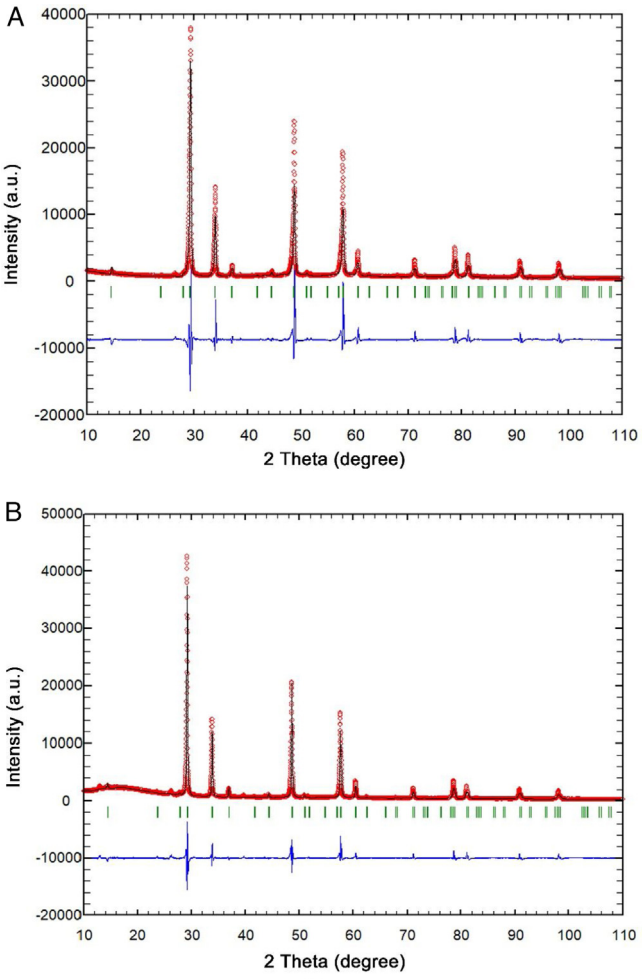

Fig. 3 – Results of the Rietveld refinement of (a) pressureless sintered, and (b) FAST-sintered $RE_2Zr_2O_7$ ceramics at 1450 °C.

ceramics possess the pyrochlore structure with the 227 space group.

Rietveld's method was employed to conduct structural refinement of the XRD patterns of samples densified by pressureless, as well as by FAST technique. The best fit between calculated and observed XRD patterns is shown in Fig. 3.

Rietveld refinement

The best fits between calculated and observed XRD patterns for two samples containing pyrochlore phase and which were sintered at 1450 °C are given in Fig. 3. All allowed Bragg reflections are shown by vertical bars. By inspecting differences between the experimental and the calculated profiles, a good agreement can be observed.

During Rietveld refinement, five different cations (La, Y, Gd, Nd, and Sm) were placed in the A cation site positions. The occupancy was set at 20% for each position. The refined unit cell parameter for the sample presented in Fig. 3a is $a = 10.5892(2)$ Å, and the coordinate of the oxygen is $x(O1) = 0.3379(8)$. The sample presented in Fig. 3b has the same structure and the cell parameter $a = 10.5999(2)$ Å, while

Please cite this article in press as: B. Matović, et al., Fabrication and characterization of high entropy pyrochlore ceramics, Bol. Soc. Esp. Cerám. Vidr. (2021), https://doi.org/10.1016/j.bsecv.2021.11.002

the coordinate of the oxygen is $x(O1) = 0.3393(7)$. The Rietveld refinement was not efficient enough in obtaining information regarding the presence and amount of each cation in the A site cation position. Five dopant cations (La, Y, Gd, Nd, and Sm) have the same 3+ oxygen number and similar ionic radii for the 8-fold coordination, according to [74]: $La^{3+} = 1.16$ Å; $Y^{3+} = 1.019$ Å; $Gd^{3+} = 1.053$ Å; $Nd^{3+} = 1.109$ Å, and $Sm^{3+} = 1.079$ Å.

In this way, the refined occupation factor cannot be considered as reliable information for the assessment of the number of cations in the A site position. The bond distances in the investigated compound were analyzed using Rietveld refinement. According to these results, Zr is surrounded by six O atoms at the same distance of 2.09 Å. Cations in position A of the pyrochlore structure are coordinated with 8 oxygen atoms with an average bond distance of 2.48 Å.

SEM and EDS analysis

The synthesized high-entropy pyrochlore powders were found to have good sinterability. Namely, as already shown, the thermal treatment at 1450 °C resulted in the achievement of densities of 93% and 98% of theoretical density, for pressureless and FAST sintering, respectively. Obtained densities show a great influence on the mechanical properties of the obtained ceramics, such as hardness. The achieved hardness in the case of conventional sintered pyrochlore is 8.3 GPa, while the FAST-obtained sample shows a hardness of 12.9 GPa. Such a significant difference can be attributed to the development of the microstructures through different densification procedures.

The microstructure of sintered samples for both sintering methods is shown in Fig. 4.

The pressureless sintered sample showed a bimodal structure with the crystal size in the range from 0.5 to 2 μm, revealing the tendency of the microparticles to coarsen during the sintering regime of 4 h at 1450 °C, Fig. 4a. It is assumed that during pressureless sintering, smaller grains are consumed by larger grains increasing in that way the average grain size. Another important feature, observed in the SEM micrographs, is the significant presence of pores through a large sample area. The pores are trapped at the polyhedral grain boundaries, as well as at the triple grain junctions.

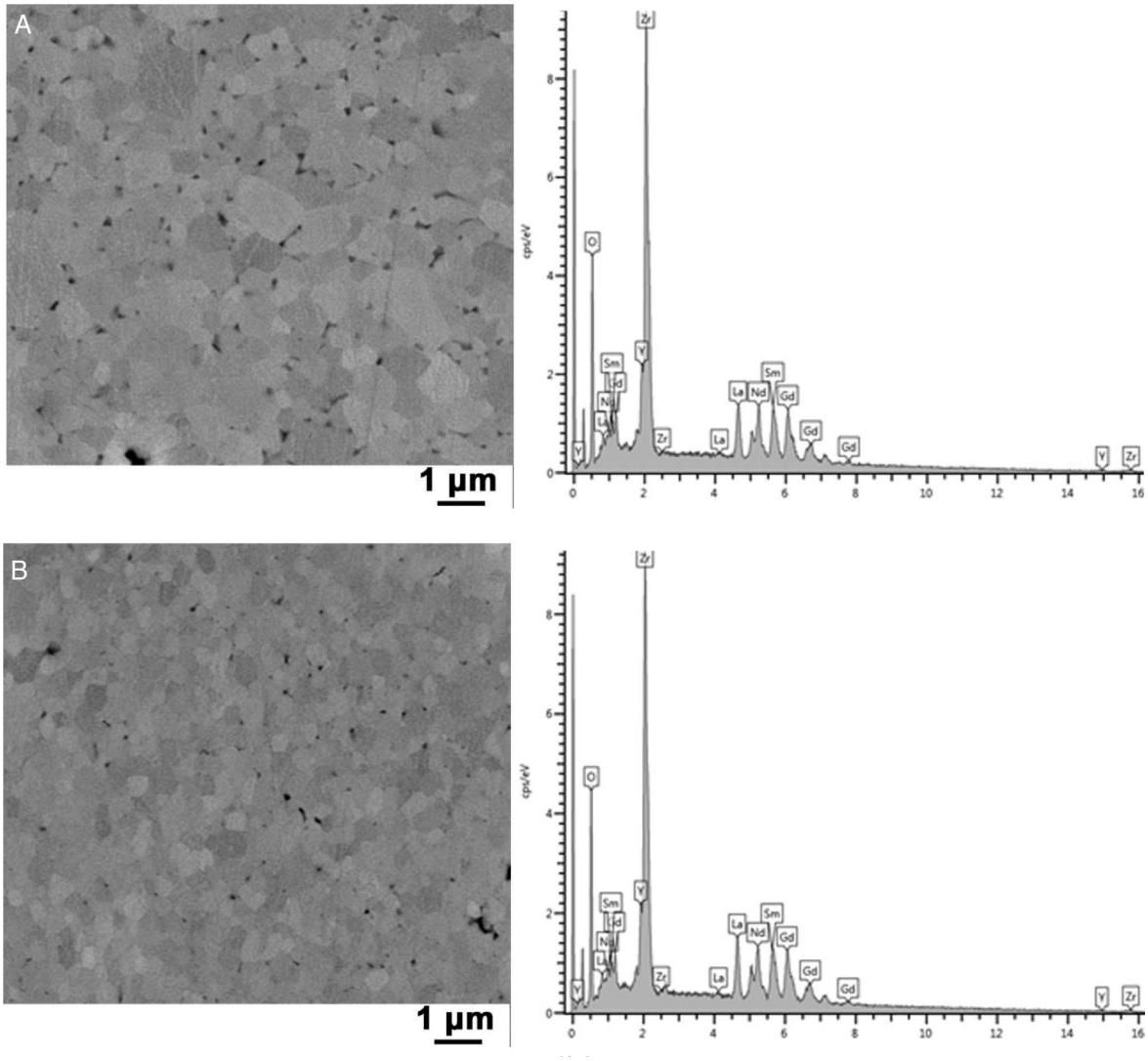

Fig. 4 – SEM micrographs and EDS spectra of (a) pressureless sintered, and (b) FAST-sintered high-entropy pyrochlore ceramics treated at 1450 °C.

Please cite this article in press as: B. Matović, et al., Fabrication and characterization of high entropy pyrochlore ceramics, Bol. Soc. Esp. Cerám. Vidr. (2021), https://doi.org/10.1016/j.bsecv.2021.11.002

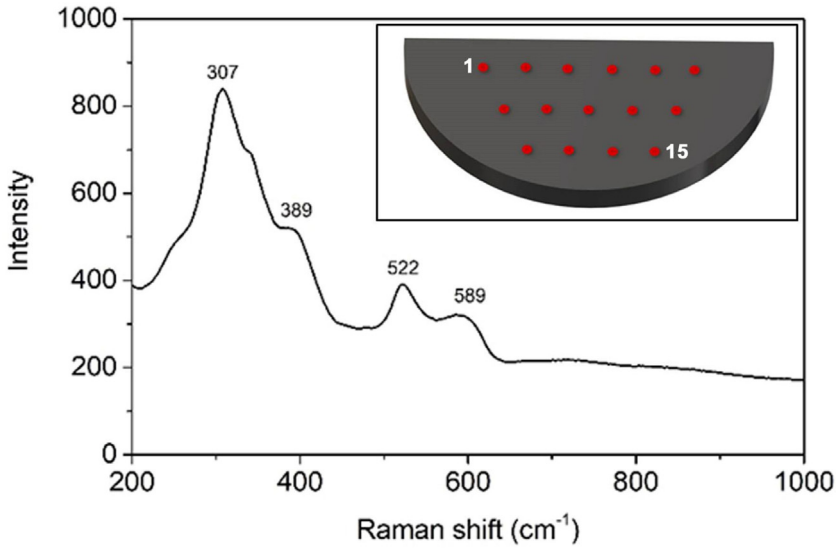

Fig. 5 – Averaged Raman spectrum of the FAST-sintered sample recorded in the range from 200 to 1000 cm^{-1} at fifteen measuring points distributed over the sample surface. The insert shows a schematic overview of the measuring points distribution on the sample surface.

On the other side, the microstructure of the FAST obtained sample exhibits densely compacted rounder-shaped grains with a narrower size distribution, Fig. 4b. The mean grain size of the FAST-sintered sample is smaller than that of the corresponding conventionally sintered grade. Namely, the grain size of this ceramic sample is in the range of 0.4–0.5 μm. The observed difference in the grain size implies that the SPS sintering has the potential to control the grain growth and homogenize the resulting microstructure due to a volumetric SPS heating mode and enhanced vacancy diffusion in this electrically conductive material. The presence of pores is also observed, but to a much lesser extent than for the conventionally sintered sample.

Qualitative EDS analysis clearly shows the presence of all elements in accordance with the nominal composition of pyrochlore, regardless of the way of their densification. The difference in the peak positions and intensities was not detected indicating the same elemental composition and their chemical stability at these temperatures in ambient atmosphere, as well as in vacuum.

Since the application of the FAST sintering technique allowed the obtainment of pyrochlore ceramic material with higher density, Raman and TEM studies were conducted only for this material.

Raman spectroscopy

Raman spectroscopy is a very sensitive technique when different pyrochlore structures are concerned. Having this in mind this analysis was carried out to observe fine domain structural changes, which cannot be done by the XRD method. Fifteen measurements were made at different positions on the sample surface. Attained results suggest that the FAST-sintered sample was homogeneous since significant differences in Raman spectra were not observed at different measuring positions.

The factor group analysis of the $A_2B_2O_7$ pyrochlore has predicted the appearance of 6 Raman active modes. From Raman spectra of the FAST-sintered sample, presented in Fig. 5, four out of the six predicted Raman bands for the Ln zirconates can be distinguished. Namely, the most intense Raman band present at 307 cm^{-1} can be ascribed to the E_g mode due to the ZrO_6 bending, two peaks observed at approximately 389 and 589 cm^{-1} could be attributed to the T_{2g} modes, while the Raman band shown at 522 cm^{-1} can be identified as the A_{1g} mode. The remaining 2 bands that correspond to the T_{2g} modes and that should be present at approximately 470 and 845 cm^{-1} were not observed [75–77].

From the XRD data shown in Figs. 2 and 3, as well as from the Raman spectrum presented in Fig. 5, it is obvious that the presented peaks are sharpened and, accordingly, it can be concluded that $Ln_2Zr_2O_7$ (Ln = La, Nd, Sm, and Gd) shows the pyrochlore structure [5].

TEM analysis

Low-magnification TEM image of the high-entropy pyrochlore sample densified by FAST at 1450 °C is shown in Fig. 6a. The TEM analysis reveals that the microstructure of this sample is composed of densely compacted micron-sized pyrochlore grains. The final ceramic material is composed mainly of grains with equiaxed morphology, where some of the grains are significantly smaller due to the high agglomeration of the starting powder. The effect of pressure applied during the FAST densification can be perceived through the destruction of present agglomerates, particle redistribution, and elimination of pores [49]. Crystalline high-entropy pyrochlore grains are in direct contact without the presence of an amorphous or secondary phase at the grain boundaries and also at the triple grain contacts. Fig. 6b shows the high-resolution TEM images of the pyrochlore grains, while the corresponding selected diffraction area is presented in Fig. 6c. If this kind

Please cite this article in press as: B. Matović, et al., Fabrication and characterization of high entropy pyrochlore ceramics, Bol. Soc. Esp. Cerám. Vidr. (2021), https://doi.org/10.1016/j.bsecv.2021.11.002

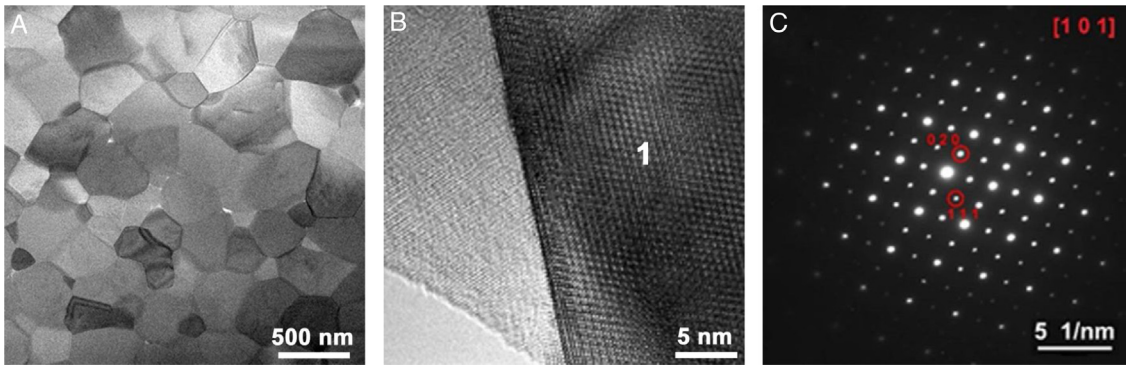

Fig. 6 – (a) STEM micrograph of the $RE_2Zr_2O_7$ ceramic sample sintered using the FAST technique at 1450 °C for 5 min, (b) HR-TEM image of two pyrochlore grains, and (c) selected area diffraction of the grain marked as 1 in the corresponding HR-TEM image presented in (b).

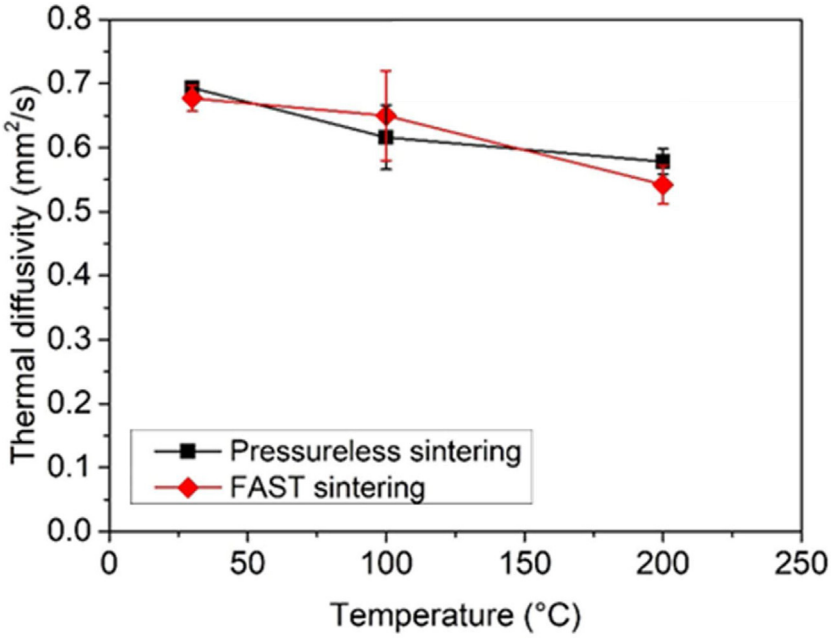

Fig. 7 – Thermal diffusivity of the pressureless sintered and FAST-sintered high-entropy pyrochlore ceramics. Error bars represent standard deviation.

of microstructure is possible to achieve during sintering at 1450 °C for only 5 min, then it is not surprising to discover that this sample possesses a high relative density (>98%). This type of the obtained microstructure provides the advantageous mechanical properties of the ceramic material, especially when the high-temperature applications are concerned.

Thermal diffusivity

One of the very important features of high-quality thermal barrier coating materials is their low thermal diffusivity. The effect of temperature on the thermal diffusivity of sintered pyrochlores is shown in Fig. 7. The thermal diffusivities of the $(La_{0.2}Y_{0.2}Gd_{0.2}Nd_{0.2}Sm_{0.2})_2Zr_2O_7$ pyrochlore system were measured for the first time. The obtained results indicate that five elements present in the A cation positions are responsible for the high scattering of phonon transport that decreases the heat conductivity. Since the porosity of material also shows a significant influence on its thermal conductivity, it was not surprising to discover that the pressureless-sintered sample, due to its higher porosity, showed a slightly lower value of thermal diffusivity in comparison to the FAST-sintered sample. Regardless of the sintering method used in the present work (pressureless sintering or FAST sintering), the recorded thermal diffusivity of high-entropy pyrochlore at room temperature was ~0.7 mm^2/s. Fabrichnaya et al. [78] also reported that thermal diffusivities for the SPS-sintered $La_2Zr_2O_7$, $Nd_2Zr_2O_7$, and $Sm_2Zr_2O_7$ pyrochlore samples were 1.13, 1.09, and 0.91 mm^2/s, respectively. Similarly, Zhang et al. [79] measured thermal diffusivities of the $(Sm_{1-x}La_x)_2Zr_2O_7$ ceramics and found that their thermal diffusivities were in the range of 0.42 – 0.96 mm^2/s, which is significantly lower than the thermal diffusivity of pure $La_2Zr_2O_7$ determined as 1.45 mm^2/s. Moreover, Zhou et al. [80] investigated the effect of rare-earth doping on the thermal properties of lanthanum zirconates and found that $La_2(Zr_{1.8}Ce_{0.2})_2O_7$, $La_{1.7}Dy_{0.3}Zr_2O_7$,

Please cite this article in press as: B. Matović, et al., Fabrication and characterization of high entropy pyrochlore ceramics, Bol. Soc. Esp. Cerám. Vidr. (2021), https://doi.org/10.1016/j.bsecv.2021.11.002

and $La_{1.7}(DyNd)_{0.15}(Zr_{0.8}Ce_{0.2})_2O_7$ had lower thermal conductivity/diffusivity than undoped $La_2Zr_2O_7$. Namely, in their work, the thermal diffusivities of doped lanthanum zirconates were reported to be in the range of 0.65–0.81 mm^2/s. Accordingly, it can be concluded that the thermal diffusivity results presented in this study are comparable to the results previously reported in the literature for the rare-earth zirconates with pyrochlore structure. Therefore, these ceramic materials, characterized by very low thermal diffusivity/conductivity, can be considered as promising candidates for thermal barrier coatings.

Conclusion

A study on the synthesis and densification of the high-entropy pyrochlore ceramics, using the combined experimental and theoretical approach, was presented.

Densification of the green compacts was achieved without the addition of sintering aids. A relative density of approximately 93% and 98%, as well as microhardness of 8.3 and 12.9 GPa were achieved by applying the pressureless and FAST sintering, respectively. The thermal diffusivity of both, pressureless and FAST-sintered, ceramics was approximately 0.5 mm^2/s. The microstructure of the obtained FAST-sintered pyrochlore ceramic exhibits low porosity with the equiaxed grains in direct contact without the presence of amorphous or secondary phases and grain size in the 0.4–0.5 μm range.

Theoretical investigations on the variable composition of ordered/disordered pyrochlore structures were performed using several different computational methods. In particular, various compositions were analyzed using the group action theory, predicted and experimentally observed pyrochlore models were generated using the PCAE and supercell approach, while the DFT-LDA structure optimization on the *ab initio* level concurs with the present XRD and Raman observations.

Conflict of interest

The authors declare that they have no known competing financial interests or personal relationships that could have appeared to influence the work reported in this paper.

Acknowledgments

This research was financially supported by the Ministry of Education, Science and Technological Development of the Republic of Serbia (Contract No. 451-03-9/2021-14/200017) and the Slovak Research and Development Agency (Contract Nos. APVV-SK-SRB-0022 and APVV-17-0328).

Appendix A. Supplementary data

Supplementary data associated with this article can be found, in the online version, at doi:10.1016/j.bsecv.2021.11.002.

REFERENCES

[1] M. Subramanian, G. Aravamudan, G.S. Rao, Oxide pyrochlores—a review, Prog. Solid State Chem. 15 (1983) 55–143.
[2] B.C. Chakoumakos, Systematics of the pyrochlore structure type, ideal $A_2B_2X_6Y$, J. Solid State Chem. 53 (1984) 120–129.
[3] L. Cai, J.C. Nino, Complex ceramic structures. I. Weberites, Acta Crystallogr. Sect. B: Struct. Sci. 65 (2009) 269–290.
[4] A. Chaudhry, A. Canning, R. Boutchko, M. Weber, N. Grønbech-Jensen, S. Derenzo, First-principles studies of Ce-doped $RE_2M_2O_7$ (RE = Y, La; M = Ti, Zr, Hf): a class of nonscintillators, J. Appl. Phys. 109 (2011) 083708.
[5] K. Shimamura, T. Arima, K. Idemitsu, Y. Inagaki, Thermophysical properties of rare-earth-stabilized zirconia and zirconate pyrochlores as surrogates for actinide-doped zirconia, Int. J. Thermophys. 28 (2007) 1074–1084.
[6] B. Matovic, J. Maletaskic, J. Zagorac, V. Pavkov, R.S. Maki, K. Yoshida, T. Yano, Synthesis and characterization of pyrochlore lanthanide (Pr, Sm) zirconate ceramics, J. Eur. Ceram. Soc. 40 (2020) 2652–2657.
[7] P.E. Blanchard, R. Clements, B.J. Kennedy, C.D. Ling, E. Reynolds, M. Avdeev, A.P. Stampfl, Z. Zhang, L.-Y. Jang, Does local disorder occur in the pyrochlore zirconates? Inorg. Chem. 51 (2012) 13237–13244.
[8] X. Cao, R. Vassen, D. Stöver, Ceramic materials for thermal barrier coatings, J. Eur. Ceram. Soc. 24 (2004) 1–10.
[9] W. Pan, S.R. Phillpot, C. Wan, A. Chernatynskiy, Z. Qu, Low thermal conductivity oxides, MRS Bull. 37 (2012) 917–922.
[10] V. Risovany, A. Zakharov, E. Muraleva, V. Kosenkov, R. Latypov, Dysprosium hafnate as absorbing material for control rods, J. Nucl. Mater. 355 (2006) 163–170.
[11] R.C. Ewing, W.J. Weber, J. Lian, Nuclear waste disposal—pyrochlore ($A_2B_2O_7$): nuclear waste form for the immobilization of plutonium and "minor" actinides, J. Appl. Phys. 95 (2004) 5949–5971.
[12] H. Yamamura, H. Nishino, K. Kakinuma, K. Nomura, Electrical conductivity anomaly around fluorite–pyrochlore phase boundary, Solid State Ionics 158 (2003) 359–365.
[13] J. Díaz-Guillén, M. Díaz-Guillén, K. Padmasree, A. Fuentes, J. Santamaría, C. León, High ionic conductivity in the pyrochlore-type $Gd_{2-y}La_yZr_2O_7$ solid solution ($0 \le y \le 1$), Solid State Ionics 179 (2008) 2160–2164.
[14] J.S. Gardner, M.J. Gingras, J.E. Greedan, Magnetic pyrochlore oxides, Rev. Mod. Phys. 82 (2010) 53.
[15] A. Zhang, M. Lü, Z. Yang, G. Zhou, Y. Zhou, Systematic research on $RE_2Zr_2O_7$ (RE = La, Nd, Eu and Y) nanocrystals: preparation, structure and photoluminescence characterization, Solid State Sci. 10 (2008) 74–81.
[16] J. Trojan-Piegza, E. Zych, M. Kosińska, Fabrication and spectroscopic properties of nanocrystalline $La_2Hf_2O_7$:Pr, Radiat. Meas. 45 (2010) 432–434.
[17] M. Uno, A. Kosuga, M. Okui, K. Horisaka, H. Muta, K. Kurosaki, S. Yamanaka, Photoelectrochemical study of lanthanide zirconium oxides, $Ln_2Zr_2O_7$ (Ln = La, Ce, Nd and Sm), J. Alloys Compd. 420 (2006) 291–297.
[18] Z. Teng, L. Zhu, Y. Tan, S. Zeng, Y. Xia, Y. Wang, H. Zhang, Synthesis and structures of high-entropy pyrochlore oxides, J. Eur. Ceram. Soc. 40 (2020) 1639–1643.
[19] S. Jiang, T. Hu, J. Gild, N. Zhou, J. Nie, M. Qin, T. Harrington, K. Vecchio, J. Luo, A new class of high-entropy perovskite oxides, Scr. Mater. 142 (2018) 116–120.
[20] T.A. Vanderah, I. Levin, M.W. Lufaso, An Unexpected Crystal-Chemical Principle for the Pyrochlore Structure, WILEY-VCH Verlag Weinheim, 2005.

Please cite this article in press as: B. Matović, et al., Fabrication and characterization of high entropy pyrochlore ceramics, Bol. Soc. Esp. Cerám. Vidr. (2021), https://doi.org/10.1016/j.bsecv.2021.11.002

[21] A.J. Wright, J. Luo, A step forward from high-entropy ceramics to compositionally complex ceramics: a new perspective, J. Mater. Sci. 55 (2020) 9812–9827.
[22] J. Xu, O. Benton, A. Islam, T. Guidi, G. Ehlers, B. Lake, Order out of a coulomb phase and higgs transition: frustrated transverse interactions of $Nd_2Zr_2O_7$, Phys. Rev. Lett. 124 (2020) 097203.
[23] A. Urban, A. Abdellahi, S. Dacek, N. Artrith, G. Ceder, Electronic-structure origin of cation disorder in transition-metal oxides, Phys. Rev. Lett. 119 (2017) 176402.
[24] O. D'yachenko, S.Y. Istomin, A. Abakumov, E. Antipov, Synthesis, structure, and properties of mixed niobium (IV, V) oxides, Inorg. Mater. 36 (2000) 247–259.
[25] Z. Wang, G. Zhou, X. Qin, F. Zhang, J. Ai, P. Liu, S. Wang, Fabrication and phase transition of $La_{2-x}Lu_xZr_2O_7$ transparent ceramics, J. Eur. Ceram. Soc. 34 (2014) 3951–3958.
[26] S. Wang, W. Li, S. Wang, Z. Chen, Synthesis of nanostructured $La_2Zr_2O_7$ by a non-alkoxide sol–gel method: from gel to crystalline powders, J. Eur. Ceram. Soc. 35 (2015) 105–112.
[27] B. Matovic, J. Maletaskic, D. Bucevac, J. Zagorac, M. Fajar, K. Yoshida, T. Yano, Synthesis, characterization and sintering of $Gd_2Hf_2O_7$ powders synthesized by solid state displacement reaction at low temperature, Ceram. Int. 44 (2018) 16972–16976.
[28] L. Kong, I. Karatchevtseva, D.J. Gregg, M.G. Blackford, R. Holmes, G. Triani, A novel chemical route to prepare $La_2Zr_2O_7$ pyrochlore, J. Am. Ceram. Soc. 96 (2013) 935–941.
[29] A.F. Fuentes, K. Boulahya, M. Maczka, J. Hanuza, U. Amador, Synthesis of disordered pyrochlores, $A_2Ti_2O_7$ (A = Y, Gd and Dy), by mechanical milling of constituent oxides, Solid State Sci. 7 (2005) 343–353.
[30] M.L. Hand, M.C. Stennett, N.C. Hyatt, Rapid low temperature synthesis of a titanate pyrochlore by molten salt mediated reaction, J. Eur. Ceram. Soc. 32 (2012) 3211–3219.
[31] T. Jeyasingh, S. Saji, P. Wariar, Synthesis of nanocrystalline $Gd_2Ti_2O_7$ by combustion process and its structural, optical and dielectric properties, in: AIP Conference Proceedings, AIP Publishing LLC, 2017, p. 020016.
[32] L. Kong, I. Karatchevtseva, D.J. Gregg, M.G. Blackford, R. Holmes, G. Triani, $Gd_2Zr_2O_7$ and $Nd_2Zr_2O_7$ pyrochlore prepared by aqueous chemical synthesis, J. Eur. Ceram. Soc. 33 (2013) 3273–3285.
[33] J. Zeng, H. Wang, Y. Zhang, M.K. Zhu, H. Yan, Hydrothermal synthesis and photocatalytic properties of pyrochlore $La_2Sn_2O_7$ nanocubes, J. Phys. Chem. C 111 (2007) 11879–11887.
[34] L. Zhou, F. Li, J.-X. Liu, Q. Hu, W. Bao, Y. Wu, X. Cao, F. Xu, G.-J. Zhang, High-entropy thermal barrier coating of rare-earth zirconate: a case study on $(La_{0.2}Nd_{0.2}Sm_{0.2}Eu_{0.2}Gd_{0.2})_2Zr_2O_7$ prepared by atmospheric plasma spraying, J. Eur. Ceram. Soc. 40 (2020) 5731–5739.
[35] S.B. Bošković, B.Z. Matovic, M.D. Vlajić, V.D. Kristić, Modified glycine nitrate procedure (MGNP) for the synthesis of SOFC nanopowders, Ceram. Int. 33 (2007) 89–93.
[36] D. Zagorac, J. Zagorac, J.C. Schön, N. Stojanović, B. Matović, ZnO/ZnS (hetero) structures: *ab initio* investigations of polytypic behavior of mixed ZnO and ZnS compounds, Acta Crystallogr. Sect. B: Struct. Sci. Cryst. Eng. Mater. 74 (2018) 628–642.
[37] R. Dovesi, A. Erba, R. Orlando, C.M. Zicovich-Wilson, B. Civalleri, L. Maschio, M. Rérat, S. Casassa, J. Baima, S. Salustro, Quantum-mechanical condensed matter simulations with CRYSTAL, Wiley Interdisc. Rev.: Comput. Mol. Sci. 8 (2018) e1360.
[38] R. Dovesi, F. Pascale, B. Civalleri, K. Doll, N.M. Harrison, I. Bush, P. D'arco, Y. Noël, M. Rérat, P. Carbonniere, The CRYSTAL code 1976-2020 and beyond, a long story, J. Chem. Phys. 152 (2020) 204111.
[39] S. Mustapha, P. D'Arco, M. De La Pierre, Y. Noël, M. Ferrabone, R. Dovesi, On the use of symmetry in configurational analysis for the simulation of disordered solids, J. Phys.: Condens. Matter 25 (2013) 105401.
[40] J.P. Perdew, A. Zunger, Self-interaction correction to density-functional approximations for many-electron systems, Phys. Rev. B 23 (1981) 5048.
[41] E. Heifets, E. Kotomin, A. Bagaturyants, J. Maier, Ab initio study of $BiFeO_3$: thermodynamic stability conditions, J. Phys. Chem. Lett. 6 (2015) 2847–2851.
[42] E. Heifets, E.A. Kotomin, A.A. Bagaturyants, J. Maier, Thermodynamic stability of stoichiometric $LaFeO_3$ and $BiFeO_3$: a hybrid DFT study, Phys. Chem. Chem. Phys. 19 (2017) 3738–3755.
[43] K. Doll, Electronic structure of GdN, and the influence of exact exchange, J. Phys.: Condens. Matter 20 (2008) 075214.
[44] J.K. Desmarais, A. Erba, R. Dovesi, Generalization of the periodic LCAO approach in the CRYSTAL code to g-type orbitals, Theor. Chem. Acc. 137 (2018) 1–11.
[45] A. Buljan, P. Alemany, E. Ruiz, Electronic structure and bonding in $CuMO_2$ (M = Al, Ga, Y) delafossite-type oxides: an *ab initio* study, J. Phys. Chem. B 103 (1999) 8060–8066.
[46] M. Towler, N. Allan, N.M. Harrison, V. Saunders, W. Mackrodt, E. Apra, Ab initio study of MnO and NiO, Phys. Rev. B 50 (1994) 5041.
[47] D. Zagorac, J. Schön, J. Zagorac, M. Jansen, Prediction of structure candidates for zinc oxide as a function of pressure and investigation of their electronic properties, Phys. Rev. B 89 (2014) 075201.
[48] B. Matović, J. Luković, D. Zagorac, O.S. Ivanova, A.E. Baranchikov, T.O. Shekunova, K.E. Yorov, O.M. Gajtko, L. Yang, M.N. Rumyantseva, Crystalline WO_3 nanoparticles for No_2 sensing, Process. Appl. Ceram. 14 (2020) 282–292.
[49] T. Bredow, M. Lerch, Anion distribution in Zr_2ON_2, Zeit. Anorg. Allg. Chem. 630 (2004) 2262–2266.
[50] H.J. Monkhorst, J.D. Pack, Special points for Brillouin-zone integrations, Phys. Rev. B 13 (1976) 5188.
[51] R. Hundt, J.C. SchoÈn, A. Hannemann, M. Jansen, Determination of symmetries and idealized cell parameters for simulated structures, J. Appl. Crystallogr. 32 (1999) 413–416.
[52] A. Hannemann, R. Hundt, J. Schön, M. Jansen, A new algorithm for space-group determination, J. Appl. Crystallogr. 31 (1998) 922–928.
[53] R. Hundt, A. Kplot, Program for Plotting and Analyzing Crystal Structures, Technicum Scientific Publishing, Stuttgart (Germany), 2016.
[54] K. Momma, F. Izumi, VESTA: a three-dimensional visualization system for electronic and structural analysis, J. Appl. Crystallogr. 41 (2008) 653–658.
[55] P. Version, 2.0. 3.0 Integrated X-ray Powder Diffraction Software, Rigaku Corporation, Tokyo, Japan, 2011, 196-8666.
[56] D. Zagorac, K. Doll, J. Schön, M. Jansen, Ab initio structure prediction for lead sulfide at standard and elevated pressures, Phys. Rev. B 84 (2011) 045206.
[57] D. Zagorac, J. Zagorac, K. Doll, M. Čebela, B. Matović, Extreme pressure conditions of BaS based materials: detailed study of structural changes, band gap engineering, elastic constants and mechanical properties, Process. Appl. Ceram. 13 (2019) 401–410.
[58] Z. Wang, G. Zhou, D. Jiang, S. Wang, Recent development of $A_2B_2O_7$ system transparent ceramics, J. Adv. Ceram. 7 (2018) 289–306.
[59] V. Sadykov, A. Shlyakhtina, N. Lyskov, E. Sadovskaya, S. Cherepanova, N. Eremeev, V. Skazka, V. Goncharov, E. Kharitonova, Oxygen diffusion in Mg-doped Sm and Gd zirconates with pyrochlore structure, Ionics 26 (2020) 4621–4633.

Please cite this article in press as: B. Matović, et al., Fabrication and characterization of high entropy pyrochlore ceramics, Bol. Soc. Esp. Cerám. Vidr. (2021), https://doi.org/10.1016/j.bsecv.2021.11.002

[60] J. Lian, L. Wang, J. Chen, K. Sun, R. Ewing, J.M. Farmer, L. Boatner, The order–disorder transition in ion-irradiated pyrochlore, Acta Mater. 51 (2003) 1493–1502.
[61] S.F. Mayer, H. Falcón, M.T. Fernández-Díaz, J.A. Alonso, The crystal structure of defect KBB'O_6 Pyrochlores (B,B': Nb,W,Sb,Te) revisited from neutron diffraction data, Crystals 8 (2018) 368.
[62] F. Zhang, M. Lang, R. Ewing, Atomic disorder in $Gd_2Zr_2O_7$ pyrochlore, Appl. Phys. Lett. 106 (2015) 191902.
[63] D.E. Vanpoucke, P. Bultinck, S. Cottenier, V. Van Speybroeck, I. Van Driessche, Density functional theory study of $La_2Ce_2O_7$: disordered fluorite versus pyrochlore structure, Phys. Rev. B 84 (2011) 054110.
[64] C. Jiang, C. Stanek, K. Sickafus, B. Uberuaga, First-principles prediction of disordering tendencies in pyrochlore oxides, Phys. Rev. B 79 (2009) 104203.
[65] Y. Li, P.M. Kowalski, G. Beridze, A.R. Birnie, S. Finkeldei, D. Bosbach, Defect formation energies in $A_2B_2O_7$ pyrochlores, Scr. Mater. 107 (2015) 18–21.
[66] B. Jiang, C.A. Bridges, R.R. Unocic, K.C. Pitike, V.R. Cooper, Y. Zhang, D.-Y. Lin, K. Page, Probing the local site disorder and distortion in pyrochlore high-entropy oxides, J. Am. Chem. Soc. (2020).
[67] D. Simeone, G.J. Thorogood, D. Huo, L. Luneville, G. Baldinozzi, V. Petricek, F. Porcher, J. Ribis, L. Mazerolles, L. Largeau, Intricate disorder in defect fluorite/pyrochlore: a concord of chemistry and crystallography, Sci. Rep. 7 (2017) 1–7.
[68] J. Shamblin, M. Feygenson, J. Neuefeind, C.L. Tracy, F. Zhang, S. Finkeldei, D. Bosbach, H. Zhou, R.C. Ewing, M. Lang, Probing disorder in isometric pyrochlore and related complex oxides, Nat. Mater. 15 (2016) 507–511.
[69] Z. Zhang, S.C. Middleburgh, M. de los Reyes, G.R. Lumpkin, B.J. Kennedy, P.E. Blanchard, E. Reynolds, L.-Y. Jang, Gradual structural evolution from pyrochlore to defect-fluorite in $Y_2Sn_{2-x}Zr_xO_7$: average vs local structure, J. Phys. Chem. C 117 (2013) 26740–26749.
[70] H.Y. Xiao, F. Gao, W.J. Weber, Ab initio investigation of phase stability of $Y_2Ti_2O_7$ and $Y_2Zr_2O_7$ under high pressure, Phys. Rev. B 80 (2009) 212102.
[71] F. Zhong, J. Zhao, L. Shi, Y. Xiao, G. Cai, Y. Zheng, J. Long, Alkaline-earth metals-doped pyrochlore $Gd_2Zr_2O_7$ as oxygen conductors for improved NO_2 sensing performance, Sci. Rep. 7 (2017) 1–10.
[72] R.R. Jitta, R. Gundeboina, N.K. Veldurthi, R. Guje, V. Muga, Defect pyrochlore oxides: as photocatalyst materials for environmental and energy applications – a review, J. Chem. Technol. Biotechnol. 90 (2015) 1937–1948.
[73] Z.G. Liu, J.H. Ouyang, Y. Zhou, J. Li, X.L. Xia, Densification, structure, and thermophysical properties of ytterbium–gadolinium zirconate ceramics, Int. J. Appl. Ceram. Technol. 6 (2009) 485–491.
[74] N. Du, X.Y. Liu, J. Narayanan, L.A. Li, M.L.M. Lim, D.Q. Li, Design of superior spider silk: from nanostructure to mechanical properties, Biophys. J. 91 (2006) 4528–4535.
[75] C. Wang, Y. Wang, Y. Cheng, W. Huang, Z.S. Khan, X. Fan, Y. Wang, B. Zou, X. Cao, Preparation and thermophysical properties of nano-sized $Ln_2Zr_2O_7$ (Ln = La, Nd, Sm, and Gd) ceramics with pyrochlore structure, J. Mater. Sci. 47 (2012) 4392–4399.
[76] B.E. Scheetz, W.B. White, Characterization of anion disorder in zirconate $A_2B_2O_7$ compounds by Raman spectroscopy, J. Am. Ceram. Soc. 62 (1979) 468–470.
[77] S. Solomon, A. George, J.K. Thomas, A. John, Preparation, characterization, and ionic transport properties of nanoscale $Ln_2Zr_2O_7$ (Ln = Ce, Pr, Nd, Sm, Gd, Dy, Er, and Yb) energy materials, J. Electron. Mater. 44 (2015) 28–37.
[78] O. Fabrichnaya, R. Wulf, M. Kriegel, G. Savinykh, M. Dopita, J. Seidel, H. Heitz, O. Nashed, U. Gross, H. Seifert, Thermophysical properties of pyrochlore and fluorite phases in the $Ln_2Zr_2O_7$-Y_2O_3 systems (Ln = La, Nd, Sm). 1. Pure pyrochlores and phases in the $Ln_2Zr_2O_7$-Y_2O_3 system, J. Alloys Compd. 586 (2014) 118–128.
[79] H. Zhang, S. Kun, X. Qiang, W. Fuchi, L. Ling, Thermal conductivity of $(Sm_{1-x}La_x)_2Zr_2O_7$ (x = 0, 0.25, 0.5, 0.75 and 1) oxides for advanced thermal barrier coatings, J. Rare Earths 27 (2009) 222–226.
[80] H. Zhou, D. Yi, Effect of rare earth doping on thermo-physical properties of lanthanum zirconate ceramic for thermal barrier coatings, J. Rare Earths 26 (2008) 770–774.

Please cite this article in press as: B. Matović, et al., Fabrication and characterization of high entropy pyrochlore ceramics, Bol. Soc. Esp. Cerám. Vidr. (2021), https://doi.org/10.1016/j.bsecv.2021.11.002